Filling Tricompartmental Ligands with Gd^{III} and Zn^{II} Ions: Some Structural and MRI Studies

Julio Corredoira-Vázquez [1], **Matilde Fondo** [1], **Jesús Sanmartín-Matalobos** [1], **Pablo Taboada** [2] **and Ana M. García-Deibe** [1,*]

[1] Department of Inorganic Chemistry, Faculty of Chemistry, Campus Vida., Universidade de Santiago de Compostela, E 15782 Santiago de Compostela, Spain; julio_corredoira@hotmail.com (J.C.-V.); matilde.fondo@usc.es (M.F.); jesus.sanmartin@usc.es (J.S.-M.)

[2] Instituto de Investigaciones Sanitarias (IDIS), Grupo de Física de Coloides y Polímeros, Departamento de Física de Partículas, Universidade de Santiago de Compostela, E 15782 Santiago de Compostela, Spain; pablo.taboada@usc.es

* Correspondence: ana.garcia.deibe@usc.es; Tel.: +34-981-814-237

Abstract: Here we report the synthesis and characterization of a mononuclear gadolinium complex (**Gd**) and two heteronuclear Zn-Gd complexes (**ZnGd** and **Zn$_2$Gd**), which contain two similar three-armed ligands that display an external compartment suitable for lanthanoid ions, and two internal compartments adequate for zinc (II) ions [H$_3$L′ = (2-(3-formyl-2-hydroxy-5-methyl phenyl)-1,3-bis[4 -(3-formyl-2-hydroxy-5-methylphenyl)-3-azabut-3-enyl]-1,3-imidazolidine; H$_3$L = 2-(5-bromo-2-hydroxy-3-methoxyphenyl)-1,3-bis[4-(5-bromo-2-hydroxy-3-methoxyphenyl)-3-azabut -3-enyl]-1,3-imidazolidine]. The synthetic methods used were varied, but the use of a metalloligand, [Zn$_2$(L)AcO], as starting material was the key factor to obtain the heterotrinuclear complex **Zn$_2$Gd**. The structure of the precursor dinuclear zinc complex is mostly preserved in this complex, since it is based on a compact [Zn$_2$Ln(L)(OH)(H$_2$O)]$^{3+}$ residue, with a μ$_3$-OH bridge between the three metal centers, which are almost forming an isosceles triangle. The asymmetric spatial arrangement of other ancillary ligands leads to chirality, what contrasts with the totally symmetric mononuclear gadolinium complex **Gd**. These features were confirmed by the crystal structures of both complexes. Despite the presence of the bulky compartmental Schiff base ligand, the chiral heterotrinuclear complex forms an intricate network which is predominately expanded in two dimensions, through varied H-bonds that connect not only the ancillary ligands, but also the nitrate counterions and some solvated molecules. In addition, some preliminary magnetic resonance imaging (MRI) studies have been made to determine the relaxivities of the three gadolinium complexes, with apparently improved T_1 and T_2 relaxivities with increasing zinc nuclearity, since both transversal and longitudinal relaxivities appear to enhance in the sequence **Gd** < **ZnGd** < **Zn$_2$Gd**.

Keywords: gadolinium; heteronuclear zinc-gadolinium complexes; chiral complex; H-bonded network; Magnetic resonance imaging (MRI); negative contrast agent

1. Introduction

Coordination chemistry of lanthanoids has experienced a considerable development in recent years, because this field is closely related to that of single-molecule magnets (SMMs) or single-ion magnets (SIMs). Their promising applications include innovative information technologies, such as molecular magnetic memories for high-density data storage, molecular quantum information processors, molecular transistors, or spintronics devices, to cite only some of their many potential applications [1].

Concurrently, a particular interest has been devoted to heteronuclear {3*d*-4*f*}-coordination complexes [2–11], this combination can lead to interesting results, since it appears that it could modulate some properties, or even afford other remarkable properties, and hence, new polyfunctional molecules could arise from this combination [10,11].

In particular, among common 3*d* ions used for these latter purposes, the combination of zinc ions with lanthanoids in heteronuclear complexes is especially significant. Thus, it appears to influence the anisotropy barrier [7,8,10–12], in some case by simple changes in the ancillary ligands [10]. Furthermore, its presence can also influence on different luminescent properties [10,11,13,14].

In this sense, we have been recently involved in a research program focused on studying hybrid Zn-Ln polynuclear complexes containing the polytopic ligands shown in Scheme 1 [15–17]. As a result of our previous work with these two ligands, we have found that complexes as {[ZnDy(HL)(NO$_3$)(OAc)(CH$_3$OH)](NO$_3$)}·1.25CH$_3$OH·0.25H$_2$O; [Zn$_2$Dy(L)(NO$_3$)$_2$(OAc)$_2$(H$_2$O)]; and [Zn$_2$Er(L)(NO$_3$)$_2$(OAc)$_2$(H$_2$O)]·1.5H$_2$O behave as field-induced single ion magnets (SIMs) [15] while [Zn$_2$Dy(L')(NO$_3$)$_3$(OH)] is a bifunctional field-induced fluorescent SIM [16]. Furthermore, we have recently presented the structure of [Zn$_2$Ho(L)(ald)(HO)(H$_2$O)(MeCN)](NO$_3$)$_2$·EtOH (Hald = 5-bromo-2-hydroxy-3-methoxy benzaldehyde) with a curious 2D H-bonded network [17].
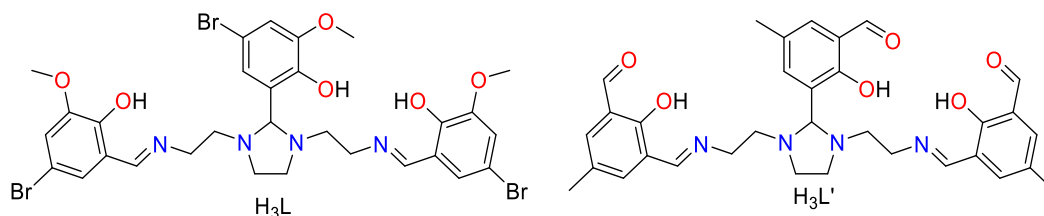
Scheme 1. Three-armed Schiff base ligands used in this work.

As an extension of this research program, we have revisited the two ligands shown in Scheme 1, with differentiated compartments for 3*d* and 4*f* metal ions, to prepare some gadolinium(III) complexes in presence, or not, of zinc(II) ions. Our aim is getting further insight into the features of these Zn-Gd compounds, although it must be mentioned that some preliminary results have been previously presented as a proceeding [18]. Thus, we have combined H$_3$L or H$_3$L' with gadolinium(III) and zinc(II) ions, in different proportions, to obtain a mononuclear gadolinium complex, as well as one heterodinuclear and one heterotrinuclear Zn-Gd complex.

Our interest, in this case study, is not focused on their magnetic behavior, since gadolinium(III) is a magnetically isotropic ion, but its ability and application as contrast agent (CAs) or zinc sensor for magnetic resonance imaging (MRI) is more than noteworthy [19–27].

This technique has been explored as a non-invasive technique that allows imaging of intact, opaque organisms in three dimensions without photobleaching or light scattering. However, MRI has relatively poor sensitivity if compared to other molecular imaging modalities, and, therefore, contrast agents (CAs) are often used to enhance imaging contrast between pathological and normal tissues. Most commonly, these are para- or superparamagnetic compounds that shorten the relaxation times of water molecules it encounters, i.e., relaxation agents. Contrast agents influence both longitudinal ($1/T_1$) and transverse ($1/T_2$) relaxation rates, and clinically approved CAs can be categorized into two main types: T_1-shortening or positive agents, and T_2-shortening or negative agents [25].

Superparamagnetic iron oxide nanoparticles (SPIONs) have been widely studied as T_2 agents, molecular complexes and nanoparticles based on Gd^{III} are commonly employed as T_1 agents [26,27]. Thus, many molecular gadolinium chelates that shorten the longitudinal relaxation time (T_1) of water protons to produce 'positive' contrast (bright) have been commercialized for their clinical use (e.g., DOTA, Dotarem, DTPA, Magnevist, ProHance), and hence, they have been widely studied [25]. However, current clinically used CAs possess relatively low contrast efficacy (relaxivity, r_1), and large amounts of these compounds have to be administered to achieve sufficient contrast, which

entails a safety concern. In fact, this concern has been recently stated by the European Agency of Medicines, which, in line with the Pharmacovigilance Risk Assessment Committee's (PRAC) March 2017 recommendations, advertises that all intravenous linear agents should be suspended [28]. Consequently, there is a current need for more efficient CAs with improved relaxivity. In this way, it has been shown that the relaxivity of some CAs can be enhanced by the presence of other species. These imaging probes are called 'smart' or responsive MR probes, and they are particularly attractive, as they modulate their relaxivity leading to signal amplification upon molecule target interaction [29–31].

Among this kind of contrast agent, some zinc(II) responsive probes have been reported since the first one described in 2001 [32], but, unfortunately, none of them show particularly large changes in r_1 relaxivity in response to zinc(II). Most of this kind of CAs are based on 1,4,7,10-tetraazacyclododecane-1,4,7,10-tetraacetic acid (DOTA), or diethylenetriaminepentaacetic acid (DTPA) derivatives, to which Gd^{3+} is coordinated, with an appended unit designed to bind Zn^{2+} ions [33–35], but less work has been done with other chelating agents. Furthermore, in spite of the numerous papers assessing gadolinium complexes as Zn^{2+} responsive imaging probes, as far as we know, heteronuclear Zn-Gd complexes have not been presented as potential MRI CAs.

Taking into account all the outlined considerations, we have made some preliminary studies to assess the longitudinal (r_1) and transverse (r_2) relaxivities of the three compounds containing gadolinium, and the results achieved are described herein.

2. Experimental

2.1. Materials and Methods

All chemical reagents were purchased from commercial sources and used as received without further purification. Elemental analysis of C, H, and N was performed on a FISONS EA 1108 analyzer. Infrared spectra were recorded in the ATR mode on a Varian 670 FT-IR spectrophotometer in the range 4000–500 cm^{-1}. X-ray powder diffraction (XRD) patterns for samples of crystallized metal complexes were measured on a Philips powder diffractometer fitted with a Philips control unit (PW1710), a vertical Philips goniometer (PW1820/00) and an Enraf Nonius generator (FR590). The instrument was equipped with a graphite diffracted beam monochromator, and a copper radiation source [λ(Kα1) = 1.5406 Å] operating at 40 kV and 30 mA. The X-ray powder diffraction patterns (XRPD) have been collected by measuring the scintillation response to Cu Kα radiation in the angular range $5 < 2\theta < 30$, with a step size of 0.02° and counting time of 4 s per step.

2.2. Synthesis of the Complexes

H_3L' (Scheme 1) was obtained in situ by template synthesis, as explained below, and previously reported [36], whilst H_3L (Scheme 1) was prepared prior to its use as described in literature [11]. This ligand was also employed to synthetize the related homodinuclear zinc(II) complex [$Zn_2(L)(OAc)$] following a method also previously reported [11].

2.2.1. Mononuclear Gd Complex

2-hydroxy-5-methyl-1,3-benzenedicarboxaldehyde (0.13 g, 0.79 mmol) solved in acetonitrile (10 mL) was added to a solution of triethylenetetramine (0.038 g, 0.26 mmol) in methanol (20 mL). The mixture was stirred for 30 min, and finally Gd(NO$_3$)$_3$·6H$_2$O (0.12 g, 0.26 mmol) was added to the obtained yellow solution. The new mixture was stirred for 4 h at room temperature and the resultant yellow solution was concentrated in a rotaevaporator, reducing its volume up to 15 mL. The solution was stored at a low temperature in the fridge, and after one day, single crystals precipitated and some of them were separated for X-ray diffraction studies. These studies demonstrated that they were of [Gd(H$_3$L′)(NO$_3$)(H$_2$O)](NO$_3$)$_2$·4H$_2$O (**Gd**). The remaining crystals were filtered and dried in air, what could have led to a partial losing of the hydration water, as it was subsequently characterized as [Gd(H$_3$L′)(NO$_3$)(H$_2$O)](NO$_3$)$_2$·2H$_2$O. In order to distinguish these crystals from the more hydrated

and fresh ones used for XRD studies, this crude crystalline solid will be named as **Gd′**. Yield: 0.087 g (34%). Elemental analysis calcd. for $C_{33}H_{42}GdN_7O_{18}$ (981.87): C 40.37, H 4.31, N 9.98%. Found: C 40.19, H 4.32, N 9.76%. FT-IR (ATR, $\tilde{\nu}/cm^{-1}$): 3271 (H_2O), 1642 (C=O), 1632 (C=N), 1305, 1281 (NO_3^-).

2.2.2. Heteronuclear Zn-Gd Complexes

$Zn(OAc)_2 \cdot 2H_2O$ (0.021 g, 0.094 mmol) was added to a chloroform (5 mL) solution of H_3L (0.074 g, 0.094 mmol). Subsequently, $Gd(NO_3)_3 \cdot 6H_2O$ (0.042, 0.094 mmol) and 5 mL of methanol were added to the resultant yellow solution. The mixture was stirred at room temperature for 2 h and a finely divided yellow powder precipitated. The solid was separated by centrifugation, dried in air, and characterized by AE, FT-IR, and X-ray diffraction studies as $ZnGd(HL)(NO_3)_2(OAc) \cdot MeOH \cdot 3H_2O$, which will be abbreviated as **ZnGd**. These reactions are summarized in Scheme 2. Yield: 0.072 g (60%). Elemental analysis calcd. for $ZnGdC_{33}H_{44}N_6O_{18}Br_3$ (1275.12): C 31.06, N 6.59, H 3.45%. Found: C 30.83, N 6.37, H 3.26%; IR spectrum (ATR, $\bar{\nu}$, cm^{-1}): 1636, 1648 (C=N); 1557 (OOC); 1285, 1300 (NO^{3-}); 3264 (OH).
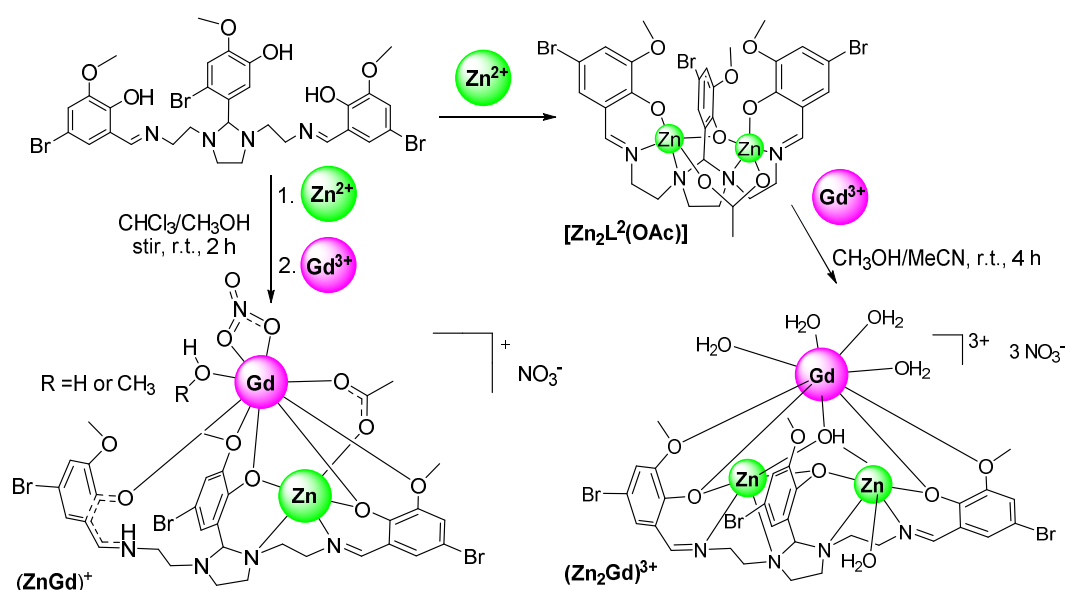
Scheme 2. Simplified synthetic routes used to prepare the heterodi- and heterotrinuclear complexes: **ZnGd** and **Zn₂Gd**. The structure of **Zn₂Gd** is based on its crystal structure, and that of **ZnGd** reflects its analogy to similar compounds X-ray characterised (see text). Solvents have been omitted for simplicity.

Many attempts of recrystallization of **ZnGd** were made in different solvents (MeOH, MeCN, CH_2Cl_2, acetone and mixtures of them), but they have only led to very small needle-like single crystals, which were not suitable to solve the crystal structure, but one of these needles (0.18 × 0.02 × 0.01 mm) diffracted enough to determine accurately the unit cell parameters: a = 10.82(3) Å, b = 16.29(5) Å, c = 26.67(7) Å, α, γ = 90, β = 97.37 (6)°, V = 4659(37) Å³, and to compare its diffraction pattern with that of its analogue $[ZnDy(HL)(NO_3)(OAc)(MeOH)](NO_3) \cdot 1.25MeOH \cdot 0.25H_2O$ [15], whose cell parameters extraordinary resemble those found for **ZnGd**. This led to comparing their calculated X-ray powder diffraction patterns, what confirmed their similitude (Figure S1 of the Supplementary Materials). This fact, among other reasons (vide infra), has led to propose the structure sketched in Scheme 2.

With the aim of obtaining a heterotrinuclear complex, a CH_3CN/CH_3OH mixture (16/8 mL) was used to solve the metalloligand $[Zn_2L(OAc)]$ (0.23 g, 0.237 mmol), and then $Gd(NO_3)_3 \cdot 6H_2O$ (0.107 g, 0.237 mmol) was added. The resulting solution was stirred at room temperature for 4 h, giving rise to a yellow precipitate. These reactions are summarized in Scheme 2. The solid was separated by centrifugation and dried in air. This solid was characterized as $[Zn_2Gd(L)(OH)(H_2O)_5]$ $(NO_3)_3 \cdot 0.75CH_3CN \cdot 3CH_3OH$. To simplify its mention, this finely divided crude but crystalline solid it will be named as **Zn₂Gd′**, to distinguish it from those crystals obtained with a slightly different

solvation. Yield: 0.136 g (39%). Elemental analysis calcd. for $Zn_2GdC_{34.5}H_{55.25}N_{7.75}O_{25.25}Br_3$ (1490.08): C, 27.78; N: 7.28; H, 3.71%. Found: C, 28.43; N, 7.35; H, 3.87%. IR (ATR, $\bar{v}$, cm^{-1}): 1635 (C=N); 1302 (NO$_3^-$); 3380 (OH).

Although the solid obtained was apparently microcrystalline, many attempts were made to obtain good quality single crystals of the heterotrinuclear compound without a totally satisfactory result. The best results were obtained from a very slow evaporation of a CH_3OH/CH_2Cl_2 solution of **Zn₂Gd′** with a little of CH_3CN yielded some crystals, which were studied with single crystal X-ray diffraction techniques although they did not diffract intensely. These studies revealed the crystal structure of $[Zn_2Gd(L)(OH)(H_2O)_5]_2(NO_3)_6 \cdot 1.5CH_3CN \cdot 2.25H_2O$, and it will be named as **Zn₂Gd** for simplicity. The similitude between **Zn₂Gd** and **Zn₂Gd′** was confirmed by the similarity of their X-ray powder diffraction patterns.

2.3. Crystal Structure Determination

In the case of **Zn₂Gd**, several crystals were selected, but despite its good appearance they were poly-twined and diffracted rather poorly. Despite this inconvenience the best data set could be used to solve and refine the crystal structure. Unfortunately, in the case of **ZnGd**, the data obtained were only useful to determine the unit cell. Diffraction data of these two complexes and those of **Gd** were collected at 100 K on a Bruker Kappa APEXII CCD diffractometer employing graphite monochromatized Mo-Kα (λ = 0.71073 Å) radiation. Multi-scan absorption corrections were applied using SADABS [37].

The structures were solved by standard direct methods, employing SHELXT [38], and then it was refined by full-matrix least-squares techniques on F^2, using SHELXL [39]. Non-hydrogen atoms, including counterions and solvated molecules, were anisotropically refined. Unfortunately, the quality of the measured data for **Zn₂Gd** was not completely satisfactory, because any crystals did not diffract very intensely. Additionally, the data collected appeared as corresponding to a poly-twinned crystal, by this was not the actual nature of this crystal, this appearance was caused by the formation of ice crystals around the crystal during the measurement, as a consequence of the low work temperature and a high humidity. Thus, these undesired reflections have interfered with the data collected for our complex. These circumstances led to refining the thermal parameters of this crystal structure with some restraints as a RIGU order, and other restrictions (ISOR and SIMU) for punctual atoms, especially those related to a particular aromatic ring (C121–C126). In addition, some relatively high residual point charges are close to heavy atoms as Br and Gd, but they appear meaningless in the model, so it could be the result of the commented undesired reflections. Some solvated molecules with partial occupation were isotropically refined.

Hydrogen atoms were mostly included in the structure factor calculations in geometrically idealized positions, but those hydrogen atoms potentially involved in classic H bonds were mostly located in Fourier maps, and then they were refined with thermal factors depending on the parent atoms. A significant effort was made to model these solvated molecules, as the H-bond scheme is remarkably intricate. Although the quality of this diffraction data is not totally satisfactory, the nature and the global spatial arrangement of the complex and other species present in the crystal appears indubitable, although the precision of some geometric parameters could be not so conclusive, therefore it will not be thoroughly discussed.

In the case of **Gd**, the central arm of the ligand is disordered on two different positions at 50%. Solvated water molecules are also very disordered, and their partial occupation sites are so low that they were isotropically treated. Despite the efforts made, no H atoms could be found, and since the H scheme was not clear they were not even considered in the final calculations. By contrast, the H atoms of the ligands could be found in Fourier maps and they were refined with thermal factors depending on the parent atoms.

Crystal data and experimental parameters relevant to the structure determinations are listed in Table S1 of the Supplementary Materials. Supplementary crystallographic data for this paper have

been deposited at Cambridge Crystallographic Data Center (CCDC-1563554 and 1570865) and can be obtained free of charge via www.ccdc.cam.ac.uk/conts/retrieving.html.

2.4. Magnetic Resonance Imaging Measurements

All studies were conducted on a 9.4 T horizontal bore magnet (Bruker BioSpin, Ettlingen, Germany) with 440 mT/m gradients and a quadrature volume coil (7 cm in diameter) or a quadrature radio-frequency transmit-receive resonator was used for data acquisition. MRI post-processing was performed using ImageJ software [40].

Agar phantoms were made following a method previously described [41] with different concentrations, ranging from 0.05 to 1.5 mM for **ZnGd** and from 0.1 to 1 mM for **Zn₂Gd′**. The relaxivity constants r_1 were calculated as the slope of the curve obtained by fitting the T_1^{-1} values versus the metal concentration in mM in water (**Gd′**) or methanol (**ZnGd** and **Zn₂Gd′**).

Weighted images were acquired using a RAREVTR sequence with 10.8 ms echo time, 6 repetition time between 900–12,000 ms and effective echo time 21.62 ms. T_2-weighted images were acquired using a multi slice multi echo sequence of 11.32 ms echo time, 3000 ms repetition time, 16 echoes, 14 slices, 1 average, field of view of 7.5 cm × 7.5 cm and matrix size of 300 × 300. In all cases, acquired images completely cover the region of interest in phantoms with 14 slices of 1 mm and in-plane resolution of 250 × 250 μm²/pixel.

3. Results and Discussion

3.1. Synthetic Method

Mononuclear **Gd** (Figure 1) was readily obtained by template synthesis, as other analogous Tb^III, Dy^III, or Er^III mononuclear complexes containing this ligand [16], by simple mixing of triethylenetetramine, 2-hydroxy-5-methyl-1,3-benzenedicarboxaldehyde, and gadolinium nitrate in 1:3:1 molar ratios. After cooling only 24 h in the fridge, single crystals of **Gd** could be isolated. In contrast, multiple attempts to isolate a similar mononuclear gadolinium(III) complex derived from H₃L were made without success. This was not surprising, as this type of three-armed ligand derived from triethylenetetramine and aromatic aldehydes is prone to yielding dinuclear lanthanoid complexes of the [Ln(L)]₂ type, with a sandwich structure [42–47].

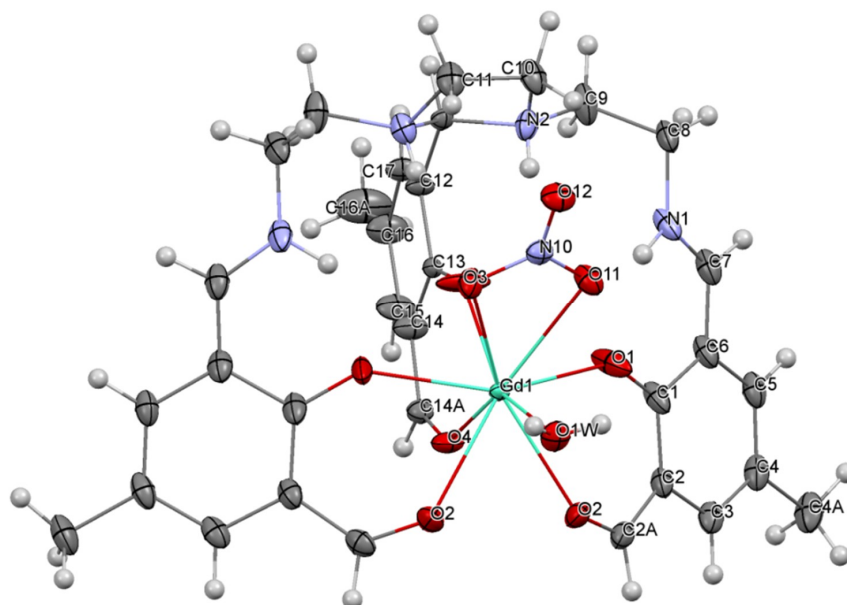**Figure 1.** Ellipsoid view of a [Gd(H₃L′)(NO₃)(H₂O)]²⁺ cation present in the unit cell of **Gd**. Only the asymmetric unit has been labelled. Counterions and solvated molecules have been omitted for clarity.

As commented, in this case, we were interested in obtaining a mononuclear gadolinium complex, and preferably with the lanthanoid ion only occupying the external compartment. Thus, the internal compartments of the ligand which are adequate for enclosing Zn^{2+} ions [36] remain uncoordinated, and the comparison with those containing one or two zinc ions could be more useful for the subsequent MRI study. In this sense, it is also remarkable that one water molecule is coordinated to the gadolinium(III) ion. This ligand was not chosen to prepare heteronuclear complexes, as no other Zn-Ln complexes could be obtained, apart from $[Zn_2Dy(L')(NO_3)_3(OH)]$, and this complex does not include coordinated water molecules, only a bridging μ_3-hydroxide ligand [16].

The synthetic method used to obtain new heteronuclear Gd-Zn complexes with H_3L, was selected according to our previous experience with this three-armed ligand [15]. Thus, without surprise, direct reaction of H_3L, $Zn(OAc)_2\cdot 2H_2O$ and $Gd(NO_3)_3\cdot 6H_2O$, both with 1:1:1 and 1:2:1 molar ratios, only led to obtaining **ZnGd** (Scheme 2), as it had also occurred when the same ligand had been combined with Er^{III}, Tb^{III}, and Dy^{III} [15].

As previously commented in the experimental section, the molecular structure of this heterodinuclear Zn-Gd complex could not be crystallographically determined, as all the single crystals obtained diffracted rather poorly. However, they diffracted enough to determine accurately the parameters of its unit cell. The values obtained for these latter one (vide supra) demonstrate that an almost total resemblance exists between these cell parameters and those previously reported for $[ZnDy(HL)(NO_3)(OAc)(MeOH)](NO_3)$ [15]. In fact, their respective volumes are 4659 and 4654 $Å^3$, respectively. This resemblance also occurs not only between their respective X-ray powder diffraction patterns, but also between their IR spectra (Figures S1 and S2 of the Supplementary Materials). Hence, they clearly appear to be isostructural. Furthermore, $[ZnDy(HL)(NO_3)(OAc)(MeOH)](NO_3)$ is also equivalent to $[ZnLn(HL)(NO_3)(OAc)(H_2O)](NO_3)$ (Ln = Er or Tb) [15], being the four complexes obtained with the same synthetic method, also employed in this case, although the crystal parameters of the two latter ones are not comparable. Consequently, only some doubt could remain about the nature of the solvent molecule coordinated to the gadolinium(III) ion, which could be methanol or water, as proposed in (Scheme 2). A similar coincidence between cell parameters exist for the already mentioned isostructural compounds $[Ln(H_3L')(NO_3)(H_2O)](NO_3)_2\cdot$complexes (Ln = Gd, Tb, Dy, Er) [16], and for other isostructural series even with different solvated molecules [48].

Likewise, after checking different synthetic routes, we had to employ the neutral homodinuclear metalloligand $[Zn_2(L)(OAc)]$, as starting material to prepare heterotrinuclear zinc-gadolinium complexes, by using a similar method to that previously employed to prepare heterotrinuclear complexes of the $[Zn_2Ln(L)(NO_3)_2(OAc)_2(H_2O)]$ type (Ln = Dy, Er) [15]. Thus, the result of mixing $[Zn_2(L)(OAc)$ with gadolinium(III) nitrate has finally allowed obtaining **Zn₂Gd** (Figure 2). However, in spite of using a similar synthetic method, this complex does not contain any coordinated acetate or nitrate ligands, but a hydroxide (O1H) ligand connecting the three metal ions, while three nitrate anions are acting as simple counterions.
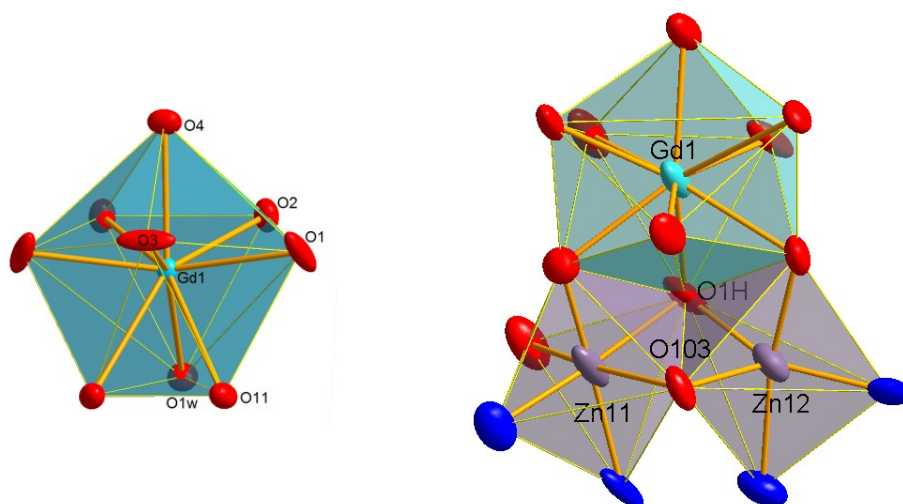
Figure 2. Ellipsoid view of one of the two $[Zn_2Gd(L)(OH)(H_2O)_5]^{3+}$ cations present in the asymmetric unit of **Zn₂Gd**. This can be considered as unit 1, so all the atoms contain a 1 as first figure in the numbering scheme. This figure shows an (*S,S,S*) enantiomer of this chiral complex. A figure of the other unit has been included in the supporting information, and it is chemically equivalent.

3.2. Coordination Environments of the Complexes

The main geometric parameters of **Gd** are collected in Table S2 of the Supplementary Materials. In the $[Gd(H_3L')(NO_3)(H_2O)]^{2+}$ cation present in **Gd** (Figure 1), the three armed ligand is neutral, so totally protonated, and it is acting as hexadentate, by using only its six O donor atoms to bind the Gd^{III} center. Accordingly, and as expected, the four the nitrogen atoms of H_3L' remain uncoordinated, but protonated in the complex, totally in the case of those of the external arms, or partially, since both imidazolidine N atoms are also holding an H atom with 50% occupation sites. Therefore, this indicates a keto more than phenol character for the O donor atoms of the three arms. This keto nature is confirmed by the C–O distances corresponding to these bonds [O(1)–C(1) and O(3)–C(13)] of about 1.29 Å (Table S2 of the Supplementary Materials) This tautomerism is not uncommon, and it can be also observed in its analogues $[Ln(H_3L')(NO_3)(H_2O)](NO_3)_2$ (Ln = Tb, Dy, Er)] [16], or those isostructural complexes similar to **ZnGd** {[ZnLn(HL)(NO_3)(OAc)(HOX)](NO_3)} (Ln = Dy, Er and Tb, X = H or Me) where one of the internal compartments also remains empty [15].

The coordination sphere of Gd^{3+} is completed by three additional oxygen atoms: two of them coming from a bidentate nitrate ligand, and one from a water molecule. This gives rise to an O_9 coordination environment, considered as a 'muffin' according to calculations made with SHAPE software [49] (Figure 3).

Figure 3. Pseudo-polyhedra formed by the coordination environments of the metal centers present in **Gd** (**left**), and in one of the cations of **Zn₂Gd** (unit 1, **right**). For heterotrinuclear complexes the two zinc(II) ions corresponding to (*S*,*S*,*S*) enantiomers have been also included.

The asymmetric unit of **Zn₂Gd** contains two chemically comparable, but crystallographically inequivalent $[Zn_2Gd(L)(OH)(H_2O)_5]^{3+}$ cations (unit 1 and unit 2). Accordingly, just an ellipsoid diagram for unit 1 is shown in Figure 2, while unit 2 is shown in Figure S3 of the Supplementary Materials. Thus, there are four units of this complex in the triclinic unit cell of **Zn₂Gd**. Main geometric parameters corresponding to this complex are listed in Table S3 of the Supplementary Materials.

Figure 2 shows that L^{3-} is acting as trinucleating in **Zn₂Gd**, with both internal N_2O compartments accommodating two zinc(II) ions. This contrasts with the only zinc atom enclosed in the dinucleating HL^{2-} entity present in **ZnGd** (Scheme 2), or in other equivalent complexes $[ZnLn(HL)(NO_3)(OAc)(ROH)](NO_3)$ (Ln = Dy, Er, Tb and R = Me or H) [15], and of course, with the two empty internal compartments observed for **Gd**.

In contrast with the pentacoordinated zinc atoms of the symmetric $[Zn_2(L)(OAc)]$ precursor, only one of the zinc atoms remains pentacoordinated (Zn12 in unit 1 and Zn22 in unit 2), while the other ones are hexacoordinated. This change is probably favored by the substitution of the μ_2-η^1:η^1 bridging acetate by a tiny μ_3-OH bridge. This distortion also leads to a significant folding of the calculated planes formed by *N*,*O*,*O*,*N* donor sets to ca. 73.4°, when it was of only ca. 26.3° in $[Zn_2(L)(OAc)]$. Furthermore, a water molecule occupies one of the apexes opposite to the central phenoxy group of L^{3-}. The values of the Addison parameter τ [50] (0.38 for Zn12 and 0.43 for Zn22) are indicative of highly distorted square pyramid geometries, where the central phenol oxygen atom occupies the apical position. In spite of this distortion, all the bond distances and angles are within normal ranges [15–17,36]. The hexacoordinated zinc atoms display pseudo-octahedral geometries (Figure 3). Different coordination numbers for the two neighboring zinc ions are also present in other related heterotrinuclear complexes of the type $[Zn_2Ln(L)(OAc)_2(NO_3)_2(H_2O)]$ (Ln = Dy, Er), but all of them contrast with the two pseudo-octahedra found around the two zinc(II) ions present in the related $[Zn_2Ho(L)(ald)(HO)(H_2O)_3(MeCN)](NO_3)_2 \cdot EtOH$ [17].

This asymmetry related to the coordination environments of the two zinc atoms leads to this complex to be chiral. As a consequence, and despite the symmetry of the three-armed H₃L ligand (Scheme 2), its central imidazolidine ring displays up to three asymmetric centers: both nitrogen atoms and the carbon atom that connects them. In both ellipsoid diagrams shown in Figure 2 and Figure S3 of the Supplementary Materials, we can see enantiomers only displaying *S* configurations for their stereocenters. Of course, although both units of the complex present in the asymmetric unit correspond coincidentally to the (*S*,*S*,*S*) enantiomer, the triclinic crystal is centrosymmetric, as it belongs to the

crystal group *P*-1, and therefore it is racemic, so that the other two units also present in the unit cell are (*R,R,R*) enantiomers.

The above described [Zn$_2$(L)(OH)(H$_2$O)] fragment of **Zn$_2$Gd** differs from the original [Zn$_2$(L)(OAc)] metalloligand used as starting material, but it is also acting as a ligand towards the Gd^{III} ion. This latter one is coordinated to the phenolate and methoxy O atoms of both external arms of the Schiff base, as well as to the hydroxide bridge. The coordination sphere of the gadolinium(III) ion is completed up to 9 by four water molecules, giving rise to a *GdO$_9$* environment (Figure 3). In this distorted *GdO$_9$* polyhedron, all the distances and angles are within their normal ranges [4,5,8,11,12,51], so this does not deserve further consideration.

The deviation of the coordination sphere with respect to an ideal nine-vertex polyhedron was calculated with the SHAPE software [49], and results indicate a muffin-like appearance, also near to a spherical capped square antiprism (Figure S2 and Table S4 in the Supplementary Materials). This muffin-like polyhedron that surrounds the gadolinium(III) ion shares one edge with each zinc pseudo-polyhedron, whilst these polyhedra around both zinc centers also share one edge (Figure 3), as occurs for [Zn$_2$Ho(L)(ald)(HO)(H$_2$O)$_3$(MeCN)](NO$_3$)$_2$·EtOH [17].

The presence of this μ_3-OH anion, which is absent in other complexes also derived from L^{3-} and [Zn$_2$(L)(OAc)] [11], lead to compare these complexes with [Zn$_2$Dy(L′)(NO$_3$)$_3$(OH)] [16]. Thus, the tight μ_3-η^1:η^1:η^1-HO$^-$ bridge leads to the three metal ions to appear as an isosceles triangle, with d(Zn···Zn), is ca. 3.0 Å, while the Zn···Ln distances are about 3.45 Å for both complexes. These intramolecular distances are similar to those found for complexes of the type [Zn$_2$Ln(L)(OAc)$_2$(NO$_3$)$_2$(H$_2$O)] (Ln = Dy^{III} and Er^{III}) [15], and for other Zn-Ln complexes with polycompartmental Schiff bases [8,9,17], and also with the 3-EtO-salen^{2-} ligand [17,52,53]. By contrast, asymmetric heterodinuclear complexes of the type of **ZnGd**, this is {[ZnLn(HL)(NO$_3$)(OAc)(HOX)](NO$_3$)} [Ln = Dy, Er and Tb, X = H or CH$_3$)], exhibit Zn···Ln distances of about 4.7 Å that are clearly longer.

3.3. Packing Schemes for the Complexes

The H-bond scheme of **Gd** is very simple. The three-armed ligand, despite being totally protonated, displays these three H atoms involved in intramolecular bonds related to imine-amine tautomerism (Figure 1). Hence, the spatial arrangement of the ligand is curiously equivalent to that shown when it is fully deprotonated and with all its compartments occupied. Only the intermolecular H bonds are connecting the coordinated water molecule to both nitrate counterions.

Contrasting with this latter scheme, the heterotrinuclear **Zn$_2$Gd** is forming a particularly intricate H bonding scheme (Table S5 and Figure S5 of the Supplementary Materials). Thus, since the quality of the diffraction data is not optimal, and in order to simplify this study, we will focus our attention mostly on classic H-bonds. In addition to classic O–H···O and some O–H···N bonds, several bifurcations, and many C–H···A interactions (A = O or Br) have been also detected (Table S5 of the Supplementary Materials).

It is evident that L^{3-}, as other related three-armed ligands, has an enwrapping character, so this partially prevents an intermolecular propagation of classic H bonds. Despite this, the coordinated water molecules and the hydroxide anion are effective H donors, so that an expansion of multiple classic O–H···O bonds occurs, and as it has been observed for [Zn$_2$Ho(L)(ald)(HO)(H$_2$O)$_3$(MeCN)](NO$_3$)$_2$·EtOH [17], this propagation curiously occurs practically with a predominately 2D arrangement, as Figure 4 shows.
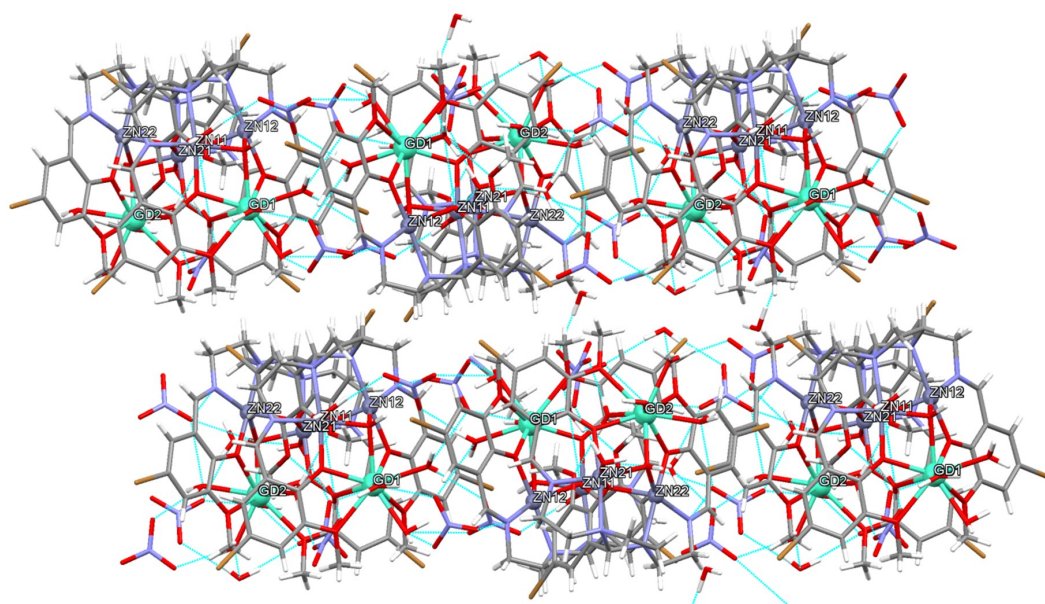
Figure 4. Balls (metals) and sticks (non-metals) view of the H-bonded layers formed by **Zn₂Gd** showing the multiple H-bonds between cations, anions and coordinated or occluded solvent molecules. Significant interactions are represented as discontinuous light blue lines. Only metal atoms have been labelled for clarity.

The frontal part of the L^{3-} ligands with the N and O donor atoms shows not only a coordinating character that encloses metal ions, but also a more hydrophilic character than its rear side [54]. In fact, this rear side, which shoes a more clearly hydrophobic nature, with the C–H bonds of imidazolidine, ethylene chains, and aromatic rings pointing towards the outside. This predominance of C–H bonds to form the surface of these layers (Figure 4 and Figure S4 of the Supplementary Materials) could influence on its solubility, as it can lead to forming extended hydrophobic surfaces that have been previously observed [17,54]. In this particular case only a few water molecules are occluded in the middle of these layers by means of an H-bond involving a solvated water molecule (O2w) and a nitrate counterion (Figure 4).

3.4. MRI Studies

The potentiality of crude solids of the three gadolinium complexes, this is: **Gd′**, **ZnGd**, and **Zn₂Gd′**, as potential MRI contrast agents was evaluated. Thus, both longitudinal r_1 and transversal r_2 relaxivities were measured, and the obtained results are summarized in Table 1, while Figure 5 shows the plots of $1/T_2$ vs. concentration of the species.

Table 1. Relaxivities for the complexes per Gd^{III} ion.

Compound	r_1 (mM^{-1} s^{-1})	r_2 (mM^{-1} s^{-1})
Gd′	0.71	29.33
ZnGd	4.90	38.63
Zn₂Gd′	7.14	84.82
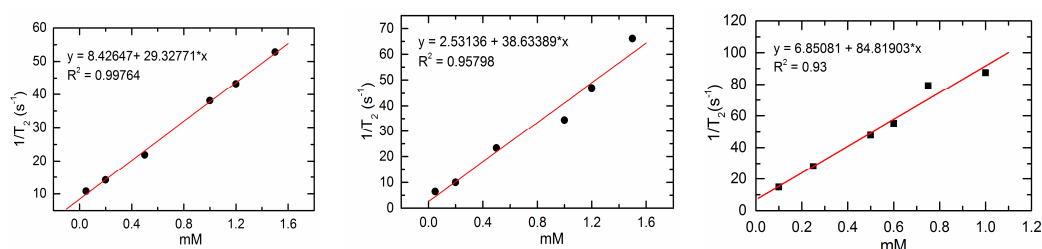
Figure 5. Plots of $1/T_2$ vs. concentration of the following species: (**left**) **Gd′**; (**middle**) **ZnGd**; and (**right**) **Zn$_2$Gd′**.

As **Gd′** is soluble in water, the longitudinal r_1 relaxivity of a water solution of **Gd′** was measured at 22 °C and 9.4 T, yielding a value of 0.71 mM^{-1} s^{-1} (Figure 5). This value demonstrates that, in spite of the nonacoordination displayed by the Gd^{3+} ion in this complex, and the presence of a water molecule in its inner sphere, even fixed by classic hydrogen bonds [55] **Gd′** shows a low r_1 relaxation and, accordingly, it is not appropriate as contrast agent.

With regard to the heteronuclear Zn-Gd complexes, the relaxometric properties of **ZnGd** and **Zn$_2$Gd′** as T_1 agents were also studied, but with a significant handicap, as both complexes are scarcely soluble in water. Consequently, the experiments were performed in methanol.

For **ZnGd**, the r_1 value of 4.90 mM^{-1} s^{-1} (Table 1) extracted from methanol solutions is comparable with those found for other commercial agents [56], so it may be considered as a potential T_1 contrast agent. Nevertheless, the r_2 value is 38.63 mM^{-1} s^{-1} (Figure 5) and, therefore, the T_1/T_2 (r_2/r_1) ratio is 7.9, a value that strongly differs from 1. As a consequence, this precludes the use of **ZnGd** as a positive MRI contrast [27]. However, the quite high r_2 value found for this heteronuclear Zn-Gd complex, in connection to the T_1/T_2 ratio higher than 6 (a condition for being used as a T_2 contrast agent), appears to indicate that it is more suitable as a negative MRI contrast, while the most usual T_2 agents were based on magnetic iron oxide nanoparticles [29]. This behavior as negative contrast appears to be confirmed by in vitro MRI experiments with agarose gel phantoms. Thus, as Figure 6 shows, the T_2-weighted phantoms show that darker images can be obtained by increasing the complex concentration.
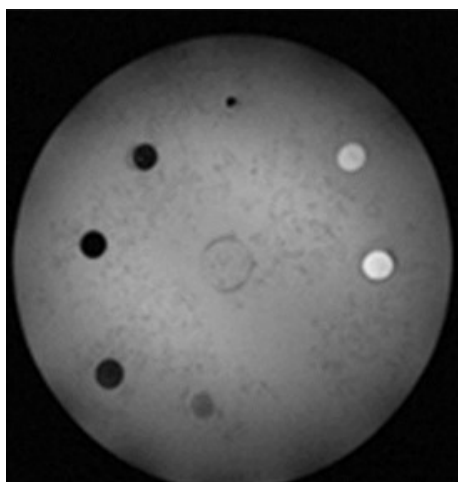

Figure 6. T_2-weighted MR image for six different increasing concentrations (clockwise) of **ZnGd** (0.05, 0.2, 0.5, 1, 1.2, and 1.5 mM), with the reference at the top center.

Similarly, the ability of **Zn$_2$Gd′** to act as potential MRI CA was also tested in methanol. In this case, the value obtained for r_1 is 7.14 mM^{-1} s^{-1}, which represents about a 150% of the relaxation time for the solution containing **ZnGd**. This result appear to suggest that an increasing Gd:Zn molar ratio in the complex could improve its relaxometric properties. The r_1 relaxivity value found of **Zn$_2$Gd′**

(7.14 mM^{-1} s^{-1}) is even higher than those values reported for some classical commercial T_1 CAs [56]. However, as occurred before, calculated r_2 value is even higher (84.83 mM^{-1} s^{-1}), while the T_1/T_2 ratio of 11.88 clearly shows that instead of a T_1 contrast, **Zn$_2$Gd′** could be proposed as a potential candidate for T_2 CA.

At this point, it should be noted that all the classical T_2 contrast agents based on superparamagnetic iron oxide nanoparticles (SPIONs) [57] have been recently forbidden, and that, currently, Ferumoxytol [58] is the only Food and Drug Administration-approved SPION that is being used as an MRI contrast agent [59]. It should be mentioned that calculated relaxivities for Ferumoxytol are r_1 38 mM^{-1} s^{-1} and r_2 83 mM^{-1} s^{-1} at 0.47 T [60]. Accordingly, the r_2 value of 84.83 mM^{-1} s^{-1} for **Zn$_2$Gd′** is even greater than the one reported for the only approved SPION MRI species.

The ability of **Zn$_2$Gd′** to act as a negative contrast has also been checked in vitro and the T_2-weighted phantom shows a progressive darkening when the concentration of complex increases (Figure 7).
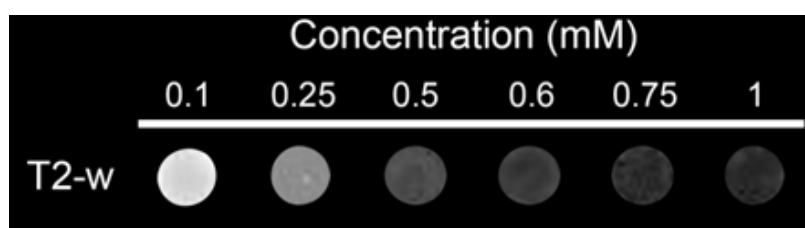
Figure 7. T_2-weighted MR image for **Zn$_2$Gd′**.

As a result of the MRI studies performed, it seems that the presence of zinc intrinsically ligated into a gadolinium complex could notably enhance the relaxometric properties of the compound, given that the heterodinuclear **ZnGd** shortens both T_1 and T_2 relaxation times. It must be noted that **ZnGd** is supposed to only contain a coordinated water molecule, as occurring for **Gd′**. This behavior is even enhanced in the case of the heterotrinuclear **Zn$_2$Gd′** complex, but in this case, there are four coordinated water molecules to the external gadolinium ion, and this fact could also contribute to increase these r values. In any case, the r_1 and r_2 values increase in the order **Gd′** < **ZnGd** < **Zn$_2$Gd′**, what could indicate that the higher the Zn:Gd molar ratio in the sample, the greater the relaxation times are.

The r_1 factors found for **ZnGd** and **Zn$_2$Gd′** are comparable or even greater than those for commercial contrast agents. Nevertheless, the T_1/T_2 ratio is in both cases even higher than 6, what indicates that they could not be used as positive, but maybe as negative contrast agents. The r_2 value for **Zn$_2$Gd′** could be comparable to that of the only SPION approved as a T_2 contrast.

It cannot be ignored that the heteronuclear Zn-Gd complexes described herein are rather insoluble in water, and, accordingly, they cannot be effective MRI agents. Nevertheless, it must be also taken into account that classical T_2 contrast agents have been mostly forbidden, due to their toxicity and fatal anaphylactic reactions. In addition, most of the T_1 CAs are also nowadays considered as potentially toxic, and consequently European Agency of Medicines is dealing with the suspension of all the classical commercial intravenous linear probes [25]. Consequently, and especially nowadays, there is a need for contributions for more efficient CAs with improved relaxivity.

Although, we are presenting herein some complexes based on linear ligands with low water solubility, a useful contribution of this work could be the presence of zinc ions in this agents accompanying to typical metal ions as gadolinium(III). This presence appears to increase the relaxation times. Although many zinc(II) responsive probes have been reported since 2001 [31], to the best of our knowledge, only two heteronuclear Zn-Gd complexes has been tested as potential contrast agents until now as T_1 agents, but not as potential negative contrasts [61,62]. Accordingly, the findings of this work could suppose an incipient contribution in the search for new CAs: the potential use of heteronuclear Zn-Gd complexes as T_2 contrast agents.

4. Conclusions

The ligands H_3L and H_3L', with differentiated compartments for $3d$ and $4f$ metal ions, allow isolating the mononuclear $[Gd(H_3L')(H_2O)(NO_3)](NO_3)_2\cdot2H_2O$ (**Gd**), heterodinuclear $\{[ZnGd(HL^2)(NO_3)(OAc)(CH_3OH)](NO_3)\}\cdot3H_2O$ (**ZnGd**), and heterotrinuclear $\{[Zn_2Gd(L^2)(OH)(H_2O)_5](NO_3)_3\}\cdot0.75CH_3CN\cdot3CH_3OH$ (**Zn₂Gd**) complexes. **Gd** could be prepared by a template method, and is totally symmetric, but the synthesis of the heteronuclear complexes needed the previous preparation of the free ligand, or even the of the metalloligand $[Zn_2(L)(OAc)]$ as a precursor. **Zn₂Gd** is chiral due to the asymmetry of the different coordination environments around the two zinc atoms.

Despite the presence of multiple and varied potential donors and acceptors for H bonding, the packing scheme of **Gd** is very simple, but that of **Zn₂Gd**—which is mostly based on classic O–H···O bonds, is intricate and basically bidimensional—and with a rather hydrophobic surface, which could affect its solubility in water.

The crystal structures of mononuclear **Gd** and heteronuclear **Zn₂Gd** demonstrate that both GdO_9 cores contain at least one water molecule coordinated to the Gd^{III} ion. The relaxometric properties of these two compounds and that of **ZnGd** were studied, with clearly different results. Thus, **Gd′**·yield low r_1 and r_2 parameters, without any interest as potential contrast agent. These r values notably increase in the sequence **Gd′** < **ZnGd** < **Zn₂Gd′**, suggesting that the relaxometric properties could improve as the Zn:Gd ratio increases. The r_1 and r_2 values, as well as the T_1/T_2 ratios indicate that **Zn₂Gd′** could be relevant as a T_2 CA, given that its r_2 value is even greater than that reported for the only approved SPION T_2 agent. Therefore, although the low solubility in water of the complexes described herein prevents their use as CAs, the findings summarized could be worthy for future design and search for new CAs, proposing heteronuclear Zn-Gd as potential candidates for T_2 MRI contrast agents.

References

1. Woodruff, D.N.; Winpenny, R.E.P.; Layfield, R.A. Lanthanide single-molecule magnets. *Chem. Rev.* **2013**, *113*, 5110–5148. [CrossRef] [PubMed]

2. Osa, S.; Kido, T.; Matsumoto, V.; Re, N.; Pochaba, A.; Mrozinski, J. A Tetranuclear 3d–4f Single Molecule Magnet: $[Cu^{II}LTb^{III}(hfac)_2]_2$. *J. Am. Chem. Soc.* **2004**, *126*, 420–421. [CrossRef] [PubMed]

3. Papatriantafyllopoulou, C.; Wernsdorfer, W.; Abboud, K.A.; Christou, G. Mn$_{21}$Dy Cluster with a Record Magnetization Reversal Barrier for a Mixed 3*d*/4*f* Single-Molecule Magnet. *Inorg. Chem.* **2011**, *50*, 421–423. [CrossRef] [PubMed]

4. Moreno Pineda, E.; Chilton, N.F.; Tuna, F.; Winpenny, R.E.P.; McInnes, E.J.L. Systematic Study of a Family of Butterfly-Like {M$_2$Ln$_2$} Molecular Magnets (M = Mg^{II}, Mn^{III}, Co^{II}, Ni^{II}, and Cu^{II}; Ln = Y^{III}, Gd^{III}, Tb^{III}, Dy^{III}, Ho^{III}, and Er^{III}). *Inorg. Chem.* **2015**, *54*, 5930–5941. [CrossRef] [PubMed]

5. Biswas, S.; Bag, P.; Das, S.; Kundu, S.; van Leusen, J.; Kögerler, P.; Chandrasekhar, V. Heterometallic [Cu$_2$Ln$_3$] (Ln = Dy^{III}, Gd^{III} and Ho^{III}) and [Cu$_4$Ln$_2$] (Ln = Dy^{III} and Ho^{III}) Compounds: Synthesis, Structure, and Magnetism. *Eur. J. Inorg. Chem.* **2017**, 1129–1142. [CrossRef]

6. Bag, P.; Chakraborty, A.; Rogez, G.; Chandrasekhar, V. Pentanuclear Heterometallic {Mn^{III}$_2$Ln$_3$} (=Gd, Dy, Tb, Ho) Assemblies in an Open-Book Type Structural Topology: Appearance of Slow Relaxation of Magnetization in the Dy(III) and Ho(III) Analogues. *Inorg. Chem.* **2014**, *53*, 6524–6533. [CrossRef] [PubMed]

7. Vignesh, K.R.; Langley, S.K.; Murray, K.S.; Rajaraman, G. Exploring the Influence of Diamagnetic Ions on the Mechanism of Magnetization Relaxation in {Co^{III}$_2$Ln^{III}$_2$} (Ln = Dy, Tb, Ho) "Butterfly" Complexes. *Inorg. Chem.* **2017**, *56*, 2518–2532. [CrossRef] [PubMed]

8. Amjad, A.; Madalan, A.M.; Andruh, M.; Caneschi, A.; Sorace, L. Slow relaxation of magnetization in an isostructural series of zinc–lanthanide complexes: An integrated EPR and AC susceptibility study. *Chem. Eur. J.* **2016**, *22*, 12849–12858. [CrossRef] [PubMed]

9. Akine, S.; Taniguchi, T.; Nabeshima, T. Helical Metallohost-Guest Complexes via Site-Selective Transmetalation of Homotrinuclear Complexes. *J. Am. Chem. Soc.* **2006**, *128*, 15765–15774. [CrossRef] [PubMed]

10. Costes, J.P.; Titos-Padilla, S.; Oyarzabal, I.; Gupta, T.; Duhayon, C.; Rajaraman, G.; Colacio, E. Effect of ligand substitution around the Dy^{III} on the SMM properties of dual-luminescent Zn–Dy and Zn–Dy–Zn complexes with large anisotropy energy barriers: A combined theoretical and experimental magnetostructural study. *Inorg. Chem.* **2016**, *55*, 4428–4440. [CrossRef] [PubMed]

11. Das, S.; Bejoymohandas, K.S.; Dey, A.; Biswas, S.; Reddy, M.L.P.; Morales, R.; Ruiz, E.; Titos-Padilla, S.; Colacio, E.; Chandrasekhar, V. Amending the Anisotropy Barrier and Luminescence Behavior of Heterometallic Trinuclear Linear [M^{II}Ln^{III}M^{II}] (Ln^{III} = Gd, Tb, Dy; M^{II} = Mg/Zn) Complexes by Change from Divalent Paramagnetic to Diamagnetic Metal Ions. *Chem. Eur. J.* **2015**, *21*, 6449–6464. [CrossRef] [PubMed]

12. Meng, Y.S.; Jiang, S.D.; Wang, B.W.; Gao, S. Understanding the Magnetic Anisotropy towards Single-Ion Magnets. *Acc. Chem. Res.* **2016**, *49*, 2381–2389. [CrossRef] [PubMed]

13. Yue, S.T.; Wei, Z.Q.; Wang, N.; Liu, W.J.; Zhao, X.; Chang, L.M.; Liu, Y.L.; Mo, H.H.; Cai, Y.P. Three novel microporous 3D heterometallic 3d–4f coordination polymers: Synthesis, crystal structures and photoluminescence properties. *Inorg. Chem. Commun.* **2011**, *14*, 1396–1399. [CrossRef]

14. Wang, Y.M.; Wang, Y.; Wang, R.X.; Qiu, J.Q.; Chi, Y.X.; Jin, J.; Niu, S.Y. Syntheses, structures and photophysical properties of a series of Zn-Ln complexes. *J. Phys. Chem. Solids* **2017**, *104*, 221–227. [CrossRef]

15. Fondo, M.; Corredoira-Vázquez, J.; García-Deibe, A.M.; Sanmartín-Matalobos, J.; Herrera, J.M.; Colacio, E. Designing Ligands to Isolate ZnLn and Zn$_2$Ln Complexes: Field-Induced Single-Ion Magnet Behavior of the ZnDy, Zn$_2$Dy, and Zn$_2$Er. *Inorg. Chem.* **2017**, *56*, 5646–5656. [CrossRef] [PubMed]

16. Fondo, M.; Corredoira-Vázquez, J.; Herrera-Lanzós, A.; García-Deibe, A.M.; Sanmartín-Matalobos, J.; Herrera, J.M.; Colacio, E.; Nuñez, C. Improving the SMM and luminescence properties of lanthanide complexes with LnO$_9$ cores in the presence of Zn^{II}: An emissive Zn$_2$Dy single ion magnet. *Dalton Trans.* **2017**, *46*, 17000–17009. [CrossRef] [PubMed]

17. Corredoira-Vázquez, J.; Fondo, M.; Sanmartín-Matalobos, J.; García-Deibe, A.M. 2D Supramolecular Structure for a Chiral Heterotrinuclear Zn^{II}$_2$Ho^{III} Complex through Varied H-Bonds Connecting Solvates and Counterions. *Proceedings* **2018**, *2*, 1114. [CrossRef]

18. Fondo, M.; Corredoira-Vázquez, J.; García-Deibe, A.; Sanmartín-Matalobos, J.; Iglesias, R.; Taboada, P. A heteronuclear ZnGd complex as a potential contrast agent for magnetic resonance imaging. In *Proceedings of the 20th International Electronic Conference on Synthetic Organic Chemistry, 1–30 November 2016*; MDPI AG: Basel, Switzerland, 2016.

19. Major, J.L.; Parigi, G.; Luchinat, C.; Meade, T.J. The synthesis and in vitro testing of a zinc-activated MRI contrast agent. *Proc. Natl. Acad. Sci. USA* **2007**, *104*, 13881–13886. [CrossRef] [PubMed]

20. Esqueda, A.C.; López, J.A.; Andreu-de-Riquer, G.; Alvarado-Monzón, J.C.; Ratnakar, J.; Lubag, A.J.M.; Sherry, A.D.; León-Rodríguez, L.M.D. A new gadolinium-based MRI zinc sensor. *J. Am. Chem. Soc.* **2009**, *131*, 11387–11391. [CrossRef] [PubMed]

21. Boros, E.; Gale, E.M.; Caravan, P. MR imaging probes: Design and applications. *Dalton Trans.* **2015**, *44*, 4804–4818. [CrossRef] [PubMed]

22. Ye, D.; Pandit, P.; Kempen, P.; Lin, J.; Xiong, L.; Sinclair, R.; Rutt, B.; Rao, J. Redox-triggered self-assembly of gadolinium-based MRI probes for sensing reducing environment. *Bioconj. Chem.* **2014**, *25*, 1526–1536. [CrossRef] [PubMed]

23. Leone, L.; Ferrauto, G.; Cossi, M.; Botta, M.; Tei, L. Optimizing the relaxivity of MRI probes at high magnetic field strengths with binuclear Gd^{III} complexes. *Front. Chem.* **2018**, *6*, 158. [CrossRef] [PubMed]

24. Nicolay, K.; Strijkers, G.; Grüll, H. Gd-Containing Nanoparticles as MRI Contrast Agents. In *The Chemistry of Contrast Agents in Medical Magnetic Resonance Imaging*, 2nd ed.; Merbach, A.E., Helm, L., Tóth, E., Eds.; John Wiley & Sons Ltd.: Hoboken, NJ, USA, 2013; pp. 449–487, ISBN 9781119991762.

25. Helm, L. Optimization of gadolinium-based MRI contrast agents for high magnetic-field applications. *Future Med. Chem.* **2010**, *2*, 385–396. [CrossRef] [PubMed]

26. Fries, P.H.; Belorizky, E. Electronic Spin Relaxation and Outer-Sphere Dynamics of Gadolinium-Based Contrast Agents. In *The Chemistry of Contrast Agents in Medical Magnetic Resonance Imaging*, 2nd ed.; Merbach, A.E., Helm, L., Tóth, E., Eds.; John Wiley & Sons Ltd.: Hoboken, NJ, USA, 2013; pp. 277–309, ISBN 9781119991762.

27. Amoroso, A.J.; Pope, S.J.A. Using lanthanide ions in molecular bioimaging. *Chem. Soc. Rev.* **2015**, *44*, 4723–4742. [CrossRef] [PubMed]

28. European Medicines Agency. PRAC Confirms Restrictions on the Use of Linear Gadolinium Agents; EMA/424715/2017. Available online: https://www.ema.europa.eu/documents/referral/gadolinium-article-31-referral-prac-confirms-restrictions-use-linear-gadolinium-agents_en.pdf (accessed on 15 November 2018).

29. Tu, C.; Osborne, E.A.; Louie, A.Y. Activatable T_1 and T_2 magnetic resonance imaging contrast agents. *Ann. Biomed. Eng.* **2011**, *39*, 1335–1348. [CrossRef] [PubMed]

30. Heffern, M.C.; Matosziuk, L.M.; Mead, T.J. Lanthanide probes for bioresponsive imaging. *Chem. Rev.* **2014**, *114*, 4496–4539. [CrossRef] [PubMed]

31. De Leon-Rodriguez, L.M.; Lubag, A.J.; Malloy, C.R.; Martinez, G.V.; Gillies, R.J.; Sherry, A.D. Responsive MRI agents for sensing metabolism in vivo. *Acc. Chem. Res.* **2009**, *42*, 948–957. [CrossRef] [PubMed]

32. Hanaoka, K.; Kikuchi, K.; Urano, Y.; Nagano, T. Selective sensing of zinc ions with a novel magnetic resonance imaging contrast agent. *J. Chem. Soc. Perkin Trans.* **2001**, *2*, 1840–1843. [CrossRef]

33. Bonnet, C.S.; Caillé, F.; Pallier, A.; Morfin, J.F.; Petoud, S.; Suzenet, F.; Tóth, E. Mechanistic studies of Gd3$^+$-based MRI contrast agents for Zn^{2+} detection: Towards rational design. *Chem. Eur. J.* **2014**, *20*, 10959–10969. [CrossRef] [PubMed]

34. Yu, J.; Martins, A.F.; Preihs, C.; Clavijo-Jordan, V.; Chirayil, S.; Zhao, P.; Wu, Y.; Nasr, K.; Kiefer, G.E.; Sherry, A.D. Amplifying the sensitivity of zinc(II) responsive MRI contrast agents by altering water exchange rates. *J. Am. Chem. Soc.* **2015**, *137*, 14173–14179. [CrossRef] [PubMed]

35. Regueiro-Figueroa, M.; Gündüz, S.; Patinec, V.; Logothetis, N.K.; Esteban-Gómez, D.; Tripier, R.; Angelovski, G.; Platas-Iglesias, C. Gd3$^+$-based magnetic resonance imaging contrast agent responsive to Zn^{2+}. *Inorg. Chem.* **2015**, *54*, 10342–10350. [CrossRef] [PubMed]

36. Fondo, M.; García-Deibe, A.M.; Ocampo, N.; Sanmartín, J.; Bermejo, M.R. Influence of some reaction conditions on the obtaining of tetra- and dinuclear zinc complexes of some Schiff bases derived from 2,6-diformyl-4-alkyl-phenols. *Polyhedron* **2008**, *27*, 2585–2594. [CrossRef]

37. Sheldrick, G.M. *SADABS, Area-Detector Absorption Correction*; Siemens Industrial Automation, Inc.: Madison, WI, USA, 2001.

38. Sheldrick, G.M. SHELXT—Integrated space-group and crystal-structure determination. *Acta Cryst.* **2015**, *A71*, 3–8. [CrossRef] [PubMed]

39. Sheldrick, G.M. Crystal structure refinement with SHELXL. *Acta Cryst.* **2015**, *C71*, 3–8. [CrossRef]

40. Schneider, C.A.; Rasband, W.S.; Eliceiri, K.W. NIH Image to ImageJ: 25 years of image analysis. *Nat. Methods* **2012**, *9*, 671. [CrossRef] [PubMed]

41. Trekker, J.; Leten, C.; Struys, T.; Lazenka, V.V.; Argibay, B.; Micholt, L.; Lambrichts, I.; Van Roy, W.; Lagae, L.; Himmelreich, U. Sensitive in vivo cell detection using size-optimized superparamagnetic nanoparticles. *Biomaterials* **2014**, *35*, 1627–1635. [CrossRef] [PubMed]

42. Yang, L.W.; Liu, S.; Wong, E.; Retting, S.J.; Orvig, C. Complexes of Trivalent Metal Ions with Potentially Heptadentate N$_4$O$_3$ Schiff Base and Amine Phenol Ligands of Varying Rigidity. *Inorg. Chem.* **1995**, *34*, 2164–2178. [CrossRef]

43. Howell, R.C.; Spence, K.V.N.; Kahwa, I.A.; Williams, D.J. Structure and luminescence of the neutral dinuclear lanthanide(III) complexes [{Ln(api)}2] {H$_3$api = 2-(2-hydroxyphenyl)-1,3-bis[4-(2-hydroxy phenyl)-3-azabut-3-enyl]-1,3-imidazolidine}. *J. Chem. Soc. Dalton Trans.* **1998**, 2727–2734. [CrossRef]

44. Chakraborty, J.; Thakurta, S.; Pilet, G.; Ziessel, R.F.; Charbonnière, L.J.; Mitra, S. Syntheses, Crystal Structures and Photophysical Properties of Two Doubly μ-Phenoxo-Bridged Ln^{III} (Ln = Pr, Nd) Homodinuclear Schiff Base Complexes. *Eur. J. Inorg. Chem.* **2009**, *2009*, 3993–4000. [CrossRef]

45. Nematirad, M.; Gee, W.J.; Langley, S.K.; Chilton, N.F.; Moubaraki, B.; Murray, K.S.; Batten, S.R. Single molecule magnetism in a μ-phenolato dinuclear lanthanide motif ligated by heptadentate Schiff base ligands. *Dalton Trans.* **2012**, *41*, 13711–13715. [CrossRef] [PubMed]

46. Zhao, L.; Wu, J.; Ke, H.; Tang, J. Three dinuclear lanthanide(III) compounds of a polydentate Schiff base ligand: Slow magnetic relaxation behaviour of the Dy^{III} derivative. *CrystEngComm* **2013**, *15*, 5301–5306. [CrossRef]

47. Xie, Q.F.; Huang, M.L.; Chen, Y.M. Bis{μ-1,3-bis[2-(5-bromo-2-oxidobenzylideneamino)ethyl]-2-(5-bromo-2-oxidophenyl)-1,3-imidazolidine}dineodymium(III) *N,N*-dimethylformamide hexasolvate. *Acta Cryst.* **2009**, *E65*, m1660. [CrossRef] [PubMed]

48. Mylonas-Margaritis, I.; Maniaki, D.; Mayans, J.; Ciammaruchi, L.; Bekiari, V.; Raptopoulou, C.P.; Psycharis, V.; Christodoulou, S.; Escuer, A.; Perlepes, S.P. Mononuclear Lanthanide(III)-Salicylideneaniline Complexes: Synthetic, Structural, Spectroscopic, and Magnetic Studies. *Magnetochemistry* **2018**, *4*, 45. [CrossRef]

49. Llunell, M.; Casanova, D.; Cirera, J.; Alemany, P.; Alvarez, S. *SHAPE: Program for the Stereochemical Analysis of Molecular Fragments by Means of Continuous Shape Measures and Associated Tools*; University of Barcelona: Barcelona, Spain, 2010.

50. Addison, A.W.; Rao, T.N.; Reedijk, J.; Van Rijk, J.; Verschoor, C.G. Synthesis, structure, and spectroscopic properties of copper(II) compounds containing nitrogen–sulphur donor ligands; the crystal and molecular structure of aqua[1,7-bis(*N*-methylbenzimidazol-2′-yl)-2,6-dithiaheptane]copper(II) perchlorate. *J. Chem. Soc. Dalton Trans.* **1984**, 1349–1356. [CrossRef]

51. Anastasiadis, N.C.; Kalofolias, D.A.; Philippidis, A.; Tzani, S.; Raptopoulou, C.P.; Psycharis, V.; Milios, C.J.; Escuer, A.; Perlepes, S.P. A family of dinuclear lanthanide(III) complexes from the use of a tridentate Schiff base. *Dalton Trans.* **2015**, *44*, 10200–10209. [CrossRef] [PubMed]

52. Maeda, M.; Hino, S.; Yamashita, K.; Kataoka, Y.; Nakano, M.; Yamamurac, T.; Kajiwara, T. Correlation between slow magnetic relaxation and the coordination structures of a family of linear trinuclear Zn(II)–Ln(III)–Zn(II) complexes (Ln = Tb, Dy, Ho, Er, Tm and Yb). *Dalton Trans.* **2012**, *41*, 13640–13648. [CrossRef] [PubMed]

53. Wong, W.K.; Liang, H.; Wong, W.Y.; Cai, Z.; Lib, K.F.; Cheah, K.W. Synthesis and near-infrared luminescence of 3d-4f bi-metallic Schiff base complexes. *New J. Chem.* **2002**, *26*, 275–278. [CrossRef]

54. García-Deibe, A.M.; Fondo, M.; Corredoira-Vázquez, J.; Fallah, M.S.E.; Sanmartín-Matalobos, J. Hierarchical assembly of antiparallel homochiral sheets formed by hydrogen-bonded helixes of a trapped-valence Co^{II}/Co^{III} complex. *Cryst. Growth Des.* **2017**, *17*, 467–473. [CrossRef]

55. Boros, E.; Srinivas, R.; Kim, H.K.; Raitsimring, A.M.; Astashkin, A.V.; Poluektov, O.G.; Niklas, J.; Horning, A.D.; Tidor, B.; Caravan, P. Intramolecular hydrogen bonding restricts Gd–aqua-ligand dynamics. *Angew. Chem. Int. Ed.* **2017**, *56*, 5603–5606. [CrossRef] [PubMed]

56. Kuda-Wedagedara, A.N.W.; Allen, M.J. Enhancing magnetic resonance imaging with contrast agents for ultra-high field strengths. *Analyst* **2014**, *139*, 4401–4410. [CrossRef] [PubMed]

57. Wang, Y.X.J. Superparamagnetic iron oxide based MRI contrast agents: Current status of clinical application. *Quant. Imaging Med. Surg.* **2011**, *1*, 35–40. [CrossRef] [PubMed]

58. Khurana, A.; Nejadnik, H.; Chapelin, F.; Lenkov, O.; Gawande, R.; Lee, S.; Gupta, S.N.; Aflakian, N.; Derugin, N.; Messing, S.; et al. Ferumoxytol: A new, clinically applicable label for stem cell tracking in arthritic joints with MRI. *Nanomedicine* **2013**, *8*, 1969–1983. [CrossRef] [PubMed]

59. Thakor, A.S.; Jokerst, J.V.; Ghanouni, P.; Campbell, J.L.; Mittra, E.; Gambhir, S.S. Clinically approved nanoparticle imaging agents. *J. Nucl. Med.* **2016**, *57*, 1833–1837. [CrossRef] [PubMed]

60. Simon, G.H.; Von Vopelius-Feldt, J.; Fu, Y.; Schlegel, J.; Pinotek, G.; Wendland, M.F.; Chen, M.H.; Daldrup-Link, H.E. Ultrasmall supraparamagnetic iron oxide-enhanced magnetic resonance imaging of antigen-induced arthritis: A comparative study between SHU 555 C, ferumoxtran-10, and ferumoxytol. *Investig. Radiol.* **2006**, *41*, 45–51. [CrossRef]

61. Schmitt, J.; Heitz, V.; Sour, A.; Bolze, F.; Kessler, P.; Flamigni, L.; Ventura, B.; Bonnet, C.S.; Toth, E. A theranostic agent combining a two-photon-absorbing photosensitizer for photodynamic therapy and a gadolinium(III) complex for MRI detection. *Chem. Eur. J.* **2016**, *22*, 2775–2786. [CrossRef] [PubMed]

62. Schmitt, J.; Jenni, S.; Sour, A.; Heitz, V.; Bolze, F.; Pallier, A.; Bonnet, C.S.; Toth, E.; Ventura, B. A porphyrin dimer–GdDOTA conjugate as a theranostic agent for one- and two-photon photodynamic therapy and MRI. *Bioconj. Chem.* **2018**. ahead of print. [CrossRef] [PubMed]